Chemistry Letters, 2026, **55**, upag006
https://doi.org/10.1093/chemle/upag006
Advance access publication 20 January 2026

Letter

Control of coffee-ring formation by vertical thermal gradients in confined droplets

Naruki Takada, Hideki Nabika*

Faculty of Science, Yamagata University, 1-4-12 Kojirakawa, Yamagata 990-8560, Japan

*Corresponding author: Faculty of Science, Yamagata University, 1-4-12 Kojirakawa, Yamagata 990-8560, Japan. Email: nabika@sci.kj.yamagata-u.ac.jp

Abstract

The coffee ring effect is a common manifestation of evaporative self-organization. Conventional strategies to control this effect, such as particle modification or surfactant addition, can be effective but often compromise the intrinsic physicochemical properties of substrates, solvents, or particles, thereby limiting their applicability. This study demonstrates a versatile route for modulating coffee-ring deposition, providing a complementary strategy for controlling evaporative self-organization in functional coatings and droplet-based material processing.

Keywords: coffee-ring, evaporative self-organization, marangoni effects.

Graphical abstract

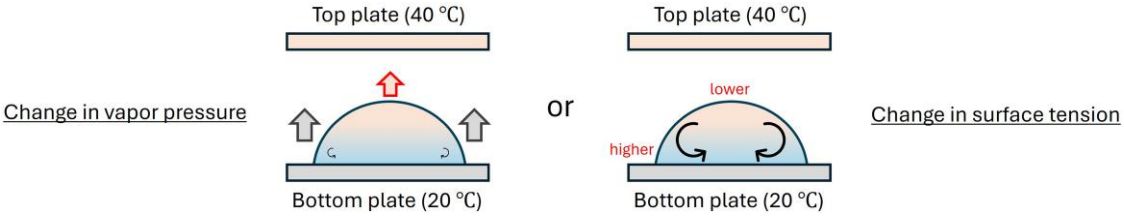

Self-organization is a hallmark of nonequilibrium systems, where macroscopic structures spontaneously emerge from interactions of microscopic components under continuous energy dissipation. Such pattern-forming processes are ubiquitous in nature, for example, Turing patterns,[1,2] the Belousov–Zhabotinsky reaction,[3,4] Bénard convection,[5,6] Liesegang patterns,[7,8] and chemical gardens.[9,10] These examples illustrate how nonequilibrium transport and reaction processes can drive spatial ordering on length scales far exceeding those of the constituent molecules or particles. Among these manifestations of dissipative self-organization, the coffee-ring effect represents a familiar phenomenon observable in everyday life, while simultaneously attracting significant fundamental and technological interest.[11–19] In particular, it has been explored in applications such as DNA chips,[20] solar cells,[21] surface-enhanced Raman scattering devices,[22,23] biosensing materials,[16,24] display technologies,[25,26] printed electronics,[27] laser-induced breakdown spectroscopy,[28] and organic solvent nanofiltration,[29] where the ring-like deposition of colloidal particles formed along the contact line of an evaporating droplet can either be exploited or must be carefully controlled. To realize such diverse functionalities, a wide variety of building blocks have been employed, including metallic nanoparticles,[16,23,30] quantum dots,[25,26] carbon nanomaterials,[27,31] MoS_2 nanosheets,[24] polymer particles,[32–34] silica particles,[35–37] coffee particles,[38] bacteria,[39] liquid crystals,[40] and salts,[41] all of which have been reported to form coffee-ring deposits under appropriate conditions.

The formation of a coffee ring is a simple process; when a solution dries on a solid surface, the solutes or particles in the solution deposit and form a ring-like deposit at the droplet periphery or along the contact line. The driving force for the accumulation of colloidal particles into a ring-like structure is an outward capillary flow that continuously transports suspended particles from the droplet center to the pinned contact line.[11,42] This flow is induced by the faster solvent evaporation at the edge compared to that at the apex due to the geometry of the liquid–air interface. Thus, contact-line pinning plays a crucial role in maintaining the radial flow throughout evaporation. The interplay among the evaporation profile, capillary circulation, contact-line dynamics, and Marangoni stresses ultimately determines the deposition morphology.

As noted above, a variety of applications have been explored, and depending on the context, coffee-ring formation

[Received on 28 November 2025; revised on 5 January 2026; accepted on 5 January 2026; corrected and typeset on 4 February 2026]

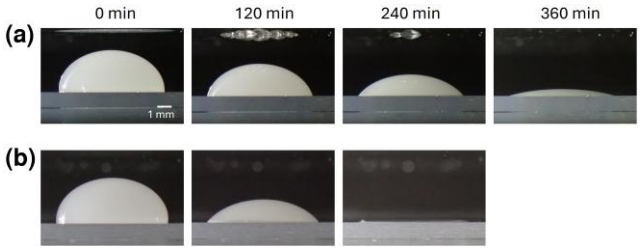

Fig. 1 Time evolution of sessile droplets confined between 2 plates. a) Lower plate at 20 °C and upper plate unheated. b) Lower plate at 20 °C and upper plate at 40 °C. The initial height of the droplet was approximately 3 mm; thus, the distance between the droplet apex and the top plate was 2 mm at the minimum inter-plate distance of 5 mm.

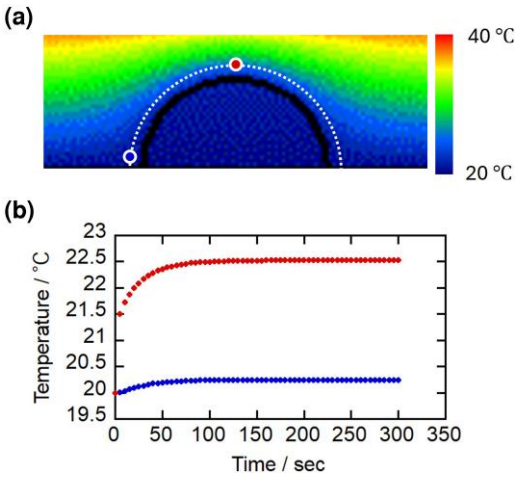

Fig. 2 Thermal simulations of confined droplet environments at lower plate at 20 °C and upper plate at 40 °C. a) Calculated temperature distribution above a droplet with $D = 5$ mm, 5 min after the onset of heating. The apex (red circle) shows an elevated gas-phase temperature relative to that of the side (blue circle). b) Temporal evolution of gas-phase temperature at the apex (red) and side (blue).

may need to be suppressed, while in other cases it can be advantageously exploited. Accordingly, numerous strategies have been developed to control coffee-ring deposition on the basis of its underlying formation mechanisms, including approaches based on substrate modification,[28,30,38] particle modification,[27,31,33,34,36,37] and the addition of chemical additives to solutions.[32,43,44] Although these approaches can effectively control coffee-ring formation, they may also compromise the intrinsic properties of the particles themselves or alter the characteristics of the resulting deposits, thereby restricting their applicability in practical applications. This challenge has motivated strategies that avoid the direct modification of system components—such as substrates, particles, or solution compositions—and instead employ indirect external interventions to control coffee-ring formation, for example, experiments with reduced gravity[41] and focused green-laser irradiation.[35]

Herein, we endeavored to establish a simpler and more versatile indirect approach. Specifically, we investigate the effect of applying a vertical thermal gradient by positioning 2 opposing thermo-plates, one above and one below an evaporating droplet. The imposed temperature gradient modified the vapor pressure distribution and surface tension at the liquid–air interface, thereby altering the balance of the capillary and Marangoni flows responsible for coffee-ring formation. Rather than targeting comprehensive control, this work suggests a new pathway toward modulating coffee-ring deposition, which can be combined with other strategies as a complementary element for controlling evaporative self-organization without perturbing the intrinsic properties of the substrate, solvent, or colloidal particles.

The configuration and other experimental and analytical protocols are described in the Supplementary Information. When the lower plate was held at 20 °C and the upper plate was not heated, the droplet height monotonically decreased with time while the footprint diameter remained essentially constant (Fig. 1a). By 360 min, only a very thin residual film remained visible. This observation indicates that drying proceeded in constant contact radius (CCR) mode, consistent with strong contact-line pinning.[35,38,44] In this mode, the droplet footprint remains fixed while evaporation progressively reduces the droplet height. As the solvent is lost, suspended particles are continuously advected toward the pinned contact line by an outward capillary flow, eventually accumulating to form a peripheral ring known as the coffee ring, as shown in Supplementary Fig. S1. When the lower plate was kept at 20 °C, and the upper plate was set to 40 °C, the droplet exhibited the same CCR mode (Fig. 1b); the footprint diameter remained constant, while the height decreased. This indicates that applying an upper hot plate did not alter the underlying drying mechanism. However, the drying kinetics accelerated, and near-complete evaporation was reached by 240 min, substantially earlier than that in the nonheated case.

To further confirm that the accelerated drying originates from thermal effects due to the upper plate, we performed finite element simulations using μ-EXCEL (Mutec Co., Ltd., Tokyo, Japan). Figure 2a shows the calculated temperature distribution for $D = 5$ mm, taken 5 min after the onset of heating. A clear vertical gradient is established above the droplet, with the air temperature near the droplet apex (red circle) elevated relative to that at the droplet side (blue circle). The temporal evolution of the local gas-phase temperature at these positions is shown in Fig. 2b. While the temperature near the side (blue) remains essentially constant at the lower plate temperature (20 °C), the temperature at the apex position (red) rapidly increases within the first 30 s and reaches an elevation of ~2.5 K above the baseline. This localized heating of the gas layer above the droplet is expected to enhance the vapor pressure gradient and thereby accelerate solvent evaporation. This interpretation is consistent with the experimental acceleration of drying observed in Fig. 1b. These simulation results support the conclusion that the reduced drying time observed in Fig. 1 arises from a heating-induced modification of the surrounding thermal environment.

Because the droplet in these experiments was confined between 2 plates, both vapor diffusion into the surrounding atmosphere and heat transfer from the upper plate were expected to be sensitive to the inter-plate spacing. This raised the possibility that the drying kinetics and deposition morphology would strongly depend on the inter-plate distance D. To examine these effects, we systematically varied D (5, 11, 15, and 30 mm) and quantified the drying time τ_{dry} and relative ring width W_{ring}. When the upper plate was not heated, τ_{dry} significantly decreased as D increased (Fig. 3a). At the smallest D of 5 mm, evaporation was significantly delayed, with the average $\tau_{dry} = 855.9$ min. In contrast, at $D > 11$ mm, τ_{dry} decreased to 200 to 400 min. As shown in Fig. 3b, a narrow

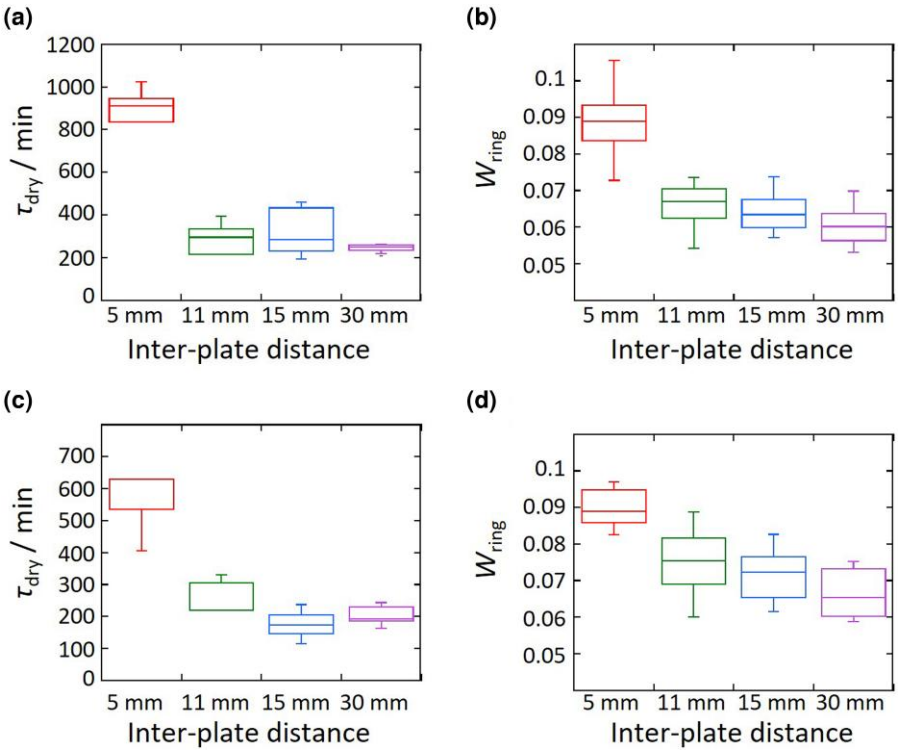

Fig. 3 Dependence of drying time τ_{dry} and relative ring width W_{ring} on the inter-plate distance D. a, b) No upper heating. c, d) With upper heating at 40 °C.

spacing ($D = 5$ mm) yielded the thickest rings, with the average $W_{ring} = 0.090$. As D increased, the rings became progressively thinner, with average W_{ring} values of 0.066, 0.064, and 0.060 for $D = 11$, 15, and 30 mm, respectively. This correlation between longer drying times and broader ring deposits is consistent with previous studies,[31] which have shown that extended evaporation provides more time for capillary-driven flows to transport suspended particles toward the pinned contact line. As a result, a greater number of particles accumulate at the droplet edge, leading to wider coffee-ring structures. Thus, the enlarged ring width observed at smaller D values can be attributed to the prolonged lifetime of outward flows under slow-drying conditions.

Heating the upper plate to 40 °C led to a slight reduction in τ_{dry} compared with the nonheated condition, with $\tau_{dry} = 200$ to 300 min for $D = 11$ to 30 mm (Fig. 3c). In contrast, for $D = 5$ mm, the average τ_{dry} significantly decreased from 855.9 min (nonheated condition) to 573.5 min. This pronounced acceleration is likely attributable to the enhanced thermal conduction through a confined air layer, which becomes significant when the upper plate is placed close to the droplet. However, the behavior of W_{ring} under heating differed from that of τ_{dry} (Fig. 3d). At $D = 5$ mm, W_{ring} remained essentially unchanged relative to that with no upper heating (average $W_{ring} = 0.090$), despite a significant decrease in τ_{dry}. Furthermore, for $D = 11$, 15, and 30 mm, the average W_{ring} increased to 0.075, 0.072, and 0.066, respectively, despite only a slight decrease in τ_{dry}. As noted above, according to the CCR mechanism, shorter drying times should result in fewer particles being transported to the contact line, leading to thinner rings. Nevertheless, at $D = 5$ mm, W_{ring} remained constant although τ_{dry} was significantly shortened, and for $D = 11$ to 30 mm, W_{ring} increased despite τ_{dry} being slightly shortened. Taken together, these findings indicate that in all cases heating promoted particle transport to the contact line, resulting in thicker rings than expected from CCR-driven dynamics alone. This clear deviation from the CCR-based trend strongly suggests the involvement of an additional heating-induced mechanism.

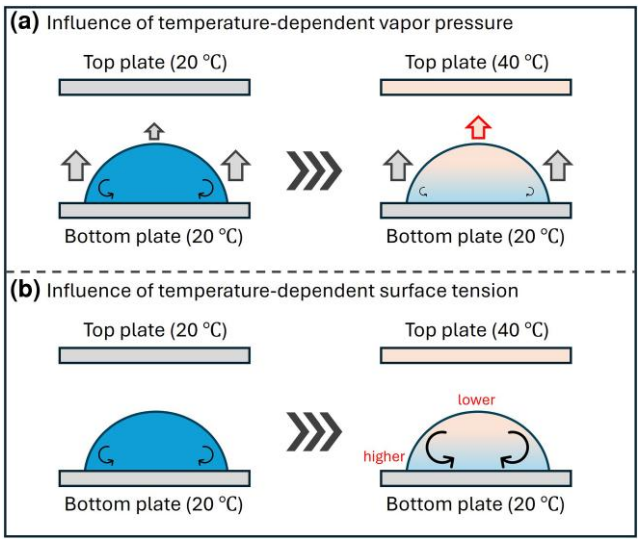

Fig. 4 Schematic of the 2 proposed heating-induced mechanisms. a) Effect of temperature-dependent vapor pressure. b) Effect of temperature-dependent surface tension.

In this study, we discuss 2 possible heating-induced pathways that can account for the observed behavior. The first mechanism is related to vapor pressure differences (Fig. 4a). Under normal conditions without heating, the Gibbs–Thomson effect leads to enhanced evaporation at the droplet

edge compared to that at the apex, establishing a vapor pressure gradient that drives outward capillary flows and particle transport toward the periphery. However, when heating is applied, simulations (Fig. 2) showed that the apex temperature rises above that at the edge, which increases the vapor pressure at the top of the droplet (right side of Fig. 4a). This can reduce the edge-to-apex vapor pressure difference and thus weaken the convective driving force. Consequently, if this mechanism dominated, heating will suppress ring formation rather than enhance it. Because our experiments reveal thicker rings under heating, this pathway is unlikely to play the primary role in the present system.

The second mechanism involves surface tension-driven Marangoni circulation (Fig. 4b). The surface tension of water decreases with increasing temperature. Therefore, the higher temperature at the droplet apex (Fig. 2) results in a relatively lower surface tension compared to that at the cooler periphery. Marangoni flow generally drives liquid motion from regions of lower surface tension to regions of higher surface tension, which in this case corresponds to circulation directed outward toward the cooler contact line. It should be noted that the CCR framework itself primarily accounts for the geometry-constrained capillary flow that transports particles to the pinned contact line. However, Marangoni circulation can concurrently act as an additional driving force, reinforcing the capillary transport dictated by the CCR drying. This mechanism is fully consistent with our observations that heating produces thicker rings even when drying times are reduced, as enhanced outward Marangoni transport compensates for the shortened evaporation period.

Taken together, these considerations suggest that enhanced surface tension-driven Marangoni flow is the primary origin of the heating-induced deviations from CCR dynamics observed for this system. While the vapor pressure effect may still play a secondary role, the predominance of interfacial tension gradients under our conditions highlights a new pathway for externally modulating evaporative self-organization. Further validation through particle tracking and localized flow field measurements is crucial and may provide a foundation for integrating this mechanism with other control strategies in practical applications. While vertical thermal gradients drive outward Marangoni flow here, extreme confinement or larger thermal gradients may flatten the vapor pressure profile, suppressing capillary flow. This interplay between Marangoni enhancement and vapor-driven suppression warrants further investigation to map deposition regimes.

We introduced a new indirect strategy for controlling coffee-ring formation by confining evaporating colloidal droplets between 2 thermo-plates. Systematic variation of the inter-plate distance D revealed that narrower gaps prolong drying and lead to thicker rings, consistent with the CCR mechanism. However, when the upper plate was heated, a clear deviation from CCR dynamics was observed; the ring widths increased, although the drying times decreased. Finite element simulations indicated that localized heating of the gas phase above the droplet accelerates evaporation, while a mechanistic analysis pointed to an enhanced surface tension-driven Marangoni flow as the dominant factor responsible for the observed thickening of rings. While the quantitative relationship between the Marangoni number and the evaporation rate remains to be fully elucidated, further studies using advanced techniques will provide more detailed insights. Further, although we attempted to visualize the internal flow in the current study, further quantification was limited by the resolution of our existing setup. However, our findings indicate that externally applied thermal fields can modulate particle transport independent of the intrinsic properties of the substrate, solvent, or particles, where the interfacial tension-driven Marangoni circulation plays a key role for tuning evaporative self-organization. This mechanism can serve as a complementary element to existing strategies, offering new opportunities for versatile control over coffee-ring deposition in practical applications.

Supplementary material

Supplementary material is available at *Chemistry Letters* online.

Funding

This work was supported by Japan Society for the Promotion of Science KAKENHI (Grant number 22H02026 and 23K23294).

Conflicts of interest

None declared.

References

1. A. Aizawa, K. Asakura, *Front. Phys.* **2024**, *12*, 1358766. https://doi.org/10.3389/fphy.2024.1358766
2. S. Kondo, T. Miura, *Science* **2010**, *329*, 1616. https://doi.org/10.1126/science.1179047
3. I. R. Epstein, V. K. Vanag, A. C. Balazs, O. Kuksenok, P. Dayal, A. Bhattacharya, *Acc. Chem. Res.* **2012**, *45*, 2160. https://doi.org/10.1021/ar200251j
4. V. K. Vanag, I. R. Epstein, *Science* **2001**, *294*, 835. https://doi.org/10.1126/science.1064167
5. A. Chatterjee, T. Ban, G. Iannacchione, *Physica A* **2022**, *593*, 126985. https://doi.org/10.1016/j.physa.2022.126985
6. T. Ban, *Entropy* **2020**, *22*, 800. https://doi.org/10.3390/e22080800
7. H. Nabika, M. Itatani, I. Lagzi, *Langmuir* **2020**, *36*, 481. https://doi.org/10.1021/acs.langmuir.9b03018
8. H. Nabika, K. Tsukada, M. Itatani, T. Ban, *Langmuir* **2022**, *38*, 11330. https://doi.org/10.1021/acs.langmuir.2c01602
9. E. Nakouzi, O. Steinbock, *Sci. Adv.* **2016**, *2*, e1601144. https://doi.org/10.1126/sciadv.1601144
10. L. M. Barge, S. S. S. Cardoso, J. H. E. Cartwright, G. J. T. Cooper, L. Cronin, A. De Wit, I. J. Doloboff, B. Escribano, R. E. Goldstein, F. Haudin, D. E. H. Jones, A. L. Mackay, J. Maselko, J. J. Pagano, J. Pantaleone, M. J. Russell, C. I. Sainz-Díaz, O. Steinbock, D. A. Stone, Y. Tanimoto, N. L. Thomas, *Chem. Rev.* **2015**, *115*, 8652. https://doi.org/10.1021/acs.chemrev.5b00014
11. R. D. Deegan, O. Bakajin, T. F. Dupont, G. Huber, S. R. Nagel, T. A. Witten, *Nature* **1997**, *389*, 827. https://doi.org/10.1038/39827
12. P. J. Yunker, T. Still, M. A. Lohr, A. G. Yodh, *Nature* **2011**, *476*, 308. https://doi.org/10.1038/nature10344
13. D. Soltman, V. Subramanian, *Langmuir* **2008**, *24*, 2224. https://doi.org/10.1021/la7026847
14. D. Mampallil, H. B. Eral, *Adv. Colloid Interface Sci.* **2018**, *252*, 38. https://doi.org/10.1016/j.cis.2017.12.008
15. W. Han, Z. Lin, *Angew. Chem. Int. Ed.* **2012**, *51*, 1534. https://doi.org/10.1002/anie.201104454

16. K. Behrouzi, Z. Khodabakhshi Fard, C.-M. Chen, P. He, M. Teng, L. Lin, *Nat. Commun.* **2025**, *16*, 4597. https://doi.org/10.1038/s41467-025-59868-y
17. M. Yang, D. Chen, J. Hu, X. Zheng, Z.-J. Lin, H. Zhu, *TrAC Trends Analyt. Chem.* **2022**, *157*, 116752. https://doi.org/10.1016/j.trac.2022.116752
18. X. Man, M. Doi, *Phys. Rev. Lett.* **2017**, *119*, 044502. https://doi.org/10.1103/PhysRevLett.119.044502
19. X. Man, M. Doi, *Phys. Rev. Lett.* **2016**, *116*, 066101. https://doi.org/10.1103/PhysRevLett.116.066101
20. V. Dugas, J. Broutin, E. Souteyrand, *Langmuir* **2005**, *21*, 9130. https://doi.org/10.1021/la050764y
21. K. Kim, J.-H. Jang, S. Hong, H. Kang, J. Lee, *J. Mater. Res. Technol.* **2024**, *31*, 3480. https://doi.org/10.1016/j.jmrt.2024.07.084
22. K. A. López-Castaños, A. Méndez-Albores, E. Quiroga-González, *Microchem. J.* **2025**, *215*, 114192. https://doi.org/10.1016/j.microc.2025.114192
23. W. Zeng, X. Fu, X. Tang, X. Liu, F. Pan, L. Wu, *Anal. Chem.* **2025**, *97*, 7429. https://doi.org/10.1021/acs.analchem.5c00215
24. Z. B. Qu, J. J. Luo, L. D. Gu, H. Q. Luo, N. B. Li, H. L. Zou, B. L. Li, *Anal. Chem.* **2025**, *97*, 18826. https://doi.org/10.1021/acs.analchem.5c03769
25. C.-Q. Lin, Z.-H. Lu, J.-P. Deng, Z.-H. Liang, J.-X. Liu, W.-Y. Cheng, H. Wang, C.-Y. Pan, *Colloids Surf. A* **2025**, *726*, 137834. https://doi.org/10.1016/j.colsurfa.2025.137834
26. K. P. Yang, J. Song, G. J. Shin, S.-H. Choi, J. H. Lee, K. Lee, *Colloids Surf. A* **2024**, *697*, 134313. https://doi.org/10.1016/j.colsurfa.2024.134313
27. H. Kim, J. I. Jang, H. H. Kim, G.-W. Lee, J. A. Lim, J. T. Han, K. Cho, *ACS Appl. Mater. Interfaces* **2016**, *8*, 3193. https://doi.org/10.1021/acsami.5b10704
28. H. Wang, H. Li, X. Huang, Z. Yao, H. Zhang, Y. H. Yao, X. Yin, Z. Chen, L. Fang, *Anal. Methods* **2024**, *17*, 64. https://doi.org/10.1039/D4AY01582G
29. C.-G. Jin, W.-H. Zhang, N. Tian, B. Wu, M.-J. Yin, Q.-F. An, *Angew. Chem. Int. Ed.* **2024**, *63*, e202405891. https://doi.org/10.1002/anie.202405891
30. Y. Han, G. Fan, Y. Han, X. Huang, W. Wang, X. Luo, Y. Zhang, L. Han, *J. Colloid Interface Sci.* **2024**, *673*, 735. https://doi.org/10.1016/j.jcis.2024.06.113
31. P. He, B. Derby, *Adv. Mater. Interfaces* **2017**, *4*, 1700944. https://doi.org/10.1002/admi.201700944
32. T. Still, P. J. Yunker, A. G. Yodh, *Langmuir* **2012**, *28*, 4984. https://doi.org/10.1021/la204928m
33. G. Hirekar, S. Shin, A. Tiwari, V. Raju, S. Singh, Y. B. Bang, S. J. Lee, A. K. Thokchom, *ACS Appl. Opt. Mater.* **2025**, *3*, 1696. https://doi.org/10.1021/acsaom.5c00166
34. K. Singh, P. Kumar, H. Raman, H. Sharma, R. Mangal, *ACS Appl. Eng. Mater.* **2025**, *3*, 275. https://doi.org/10.1021/acsaenm.4c00785
35. P. Han, L. J. Yang, Z. Zhu, X. Liang, W. Wu, *ACS Omega* **2025**, *10*, 35785. https://doi.org/10.1021/acsomega.5c02579
36. S. H. Kim, Y. Huh, B. S. Park, K. I. Jung, Y.-Y. Won, J. Bang, H. W. Jung, *Chem. Eng. J.* **2024**, *494*, 152929. https://doi.org/10.1016/j.cej.2024.152929
37. M. Rey, J. Walter, J. Harrer, C. M. Perez, S. Chiera, S. Nair, M. Ickler, A. Fuchs, M. Michaud, M. J. Uttinger, A. B. Schofield, J. H. J. Thijssen, M. Distaso, W. Peukert, N. Vogel, *Nat. Commun.* **2022**, *13*, 2840. https://doi.org/10.1038/s41467-022-30497-z
38. Y. J. Han, M. S. Kim, S. M. Yoon, S. N. Yoon, W. Y. Kim, S. Kim, Y. T. Cho, *Molecules* **2025**, *30*, 3146. https://doi.org/10.3390/molecules30153146
39. K. K. Dewangan, SRS,D Roy, A. R. Chowdhury, D. Chakravortty, S. Basu, *Langmuir* **2025**, *41*, 8252. https://doi.org/10.1021/acs.langmuir.5c00058
40. Z. S. Davidson, Y. Huang, A. Gross, A. Martinez, T. Still, C. Zhou, P. J. Collings, R. D. Kamien, A. G. Yodh, *Nat. Commun.* **2017**, *8*, 15642. https://doi.org/10.1038/ncomms15642
41. R. Hadidi, V. D. Pinckney, S. A. Shaw, O. Steinbock, B. B. Dangi, *J. Phys. Chem. B* **2025**, *129*, 3028. https://doi.org/10.1021/acs.jpcb.4c06963
42. J. R. Trantum, Z. E. Eagleton, C. A. Patil, J. M. Tucker-Schwartz, M. L. Baglia, M. C. Skala, F. R. Haselton, *Langmuir* **2013**, *29*, 6221. https://doi.org/10.1021/la400542x
43. M. Anyfantakis, Z. Geng, M. Morel, S. Rudiuk, D. Baigl, *Langmuir* **2015**, *31*, 4113. https://doi.org/10.1021/acs.langmuir.5b00453
44. N. S. Howard, A. J. Archer, D. N. Sibley, D. J. Southee, K. G. U. Wijayantha, *Langmuir* **2023**, *39*, 929. https://doi.org/10.1021/acs.langmuir.2c01691